The Hutlets - a biorthogonal wavelet family and their high speed implementation with RNS, multiplier-free, perfect reconstruction QMF

U. Meyer-Bäse[a,b] and F. Taylor[b]

[a]Institut of Digital Technics, TU Darmstadt
64283 Darmstadt, Germany

[b]High Speed Digital Architecture Laboratory,
University of Florida,Gainesville, Florida 32611 USA

ABSTRACT

The relationship between wavelets, Laplace pyramids and QMF are now well established.[1–3] In recent years biorthorgonal wavelets have become of increased interest because, compared with orthogonal wavelets, they are symmetric and linear phase. In this paper the Hut † function[4] is used as a scaling function (father wavelet) to construct a biorthogonal wavelet family, we call Hutlets. A realization with perfect reconstruction, multiplier- free quadrature mirror filters using RNS technic is proposed. The approximation-filter is a CIC lowpass, the detail-filter is a CHPC highpass, and the reconstruction filters are IIRs. Exact pole-zero annihilation is guaranteed by implementing polynomial filters, over an integer ring, in the residue arithmetic system (RNS). Since CIC and CHPC designs rely on the exact annihilation of selected poles-zeros, a new facilitating technology is required which is fast, compact, and numerically exact. How this can be achieved is the thrust of this paper. An application of the Hutlets to pulse amplitude modulated signals is explained.

Keywords: Biorthogonal Wavelets, Quadrature Mirror Filter (QMF), Residue Number System (RNS)

1. INTRODUCTION

The Hut function $h(t)$, first defined by W. Hilberg in 1971,[4] has a total length T and is an infinite convolution product (symbol *) of rectangles with area one and of length $T/2, T/4, T/8, \ldots$:

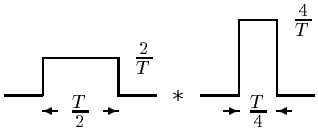

$$* \cdots * \; \delta(t) = h(t) \qquad \longleftrightarrow \quad H(\omega) = \prod_{i=1}^{+\infty} \operatorname{sinc}\left(2^{-i}\omega T/2\right), \tag{1}$$

where $\operatorname{sinc}(x) = \sin(x)/x$. Figure 1 shows the Hut and a triangular function along with their spectra. There is a second, less complicated algorithm to construct the Hut function using the Morse Thue Sequence (MTS). We use 2^N sequence values of the MTS, were we use a -1 instead of zero, and integrate this sequence N times. Figure 2(a) shows this construction for 64 MTS values. The discrete values are for graphical purpose connected by a step functions. For $N \to \infty$ we have then the Hut function. Appendix A shows some more functional approximation of the Hut function. The MTS can be easily constructed. Three rules are common known[5,6]:

1) *(Parity)* The integers $\mathbb{Z}$ are written in binary notation and the odd parity is computed: $p(0) = 1, p(1) = 0, p(2) = 0, p(3) = 1, p(4) = 0, \ldots$

Tel.: 352-392-2692; Fax: 352-392-0044
Email: {uwe,fjt}@alpha.ee.ufl.edu
Paper-location-URL: http://www.dtro.e-technik.th-darmstadt.de/umb/papers
Supported by the German DFG under grant ME1419/2-1.
† "Hut" is the German equivalent for the English "hat".

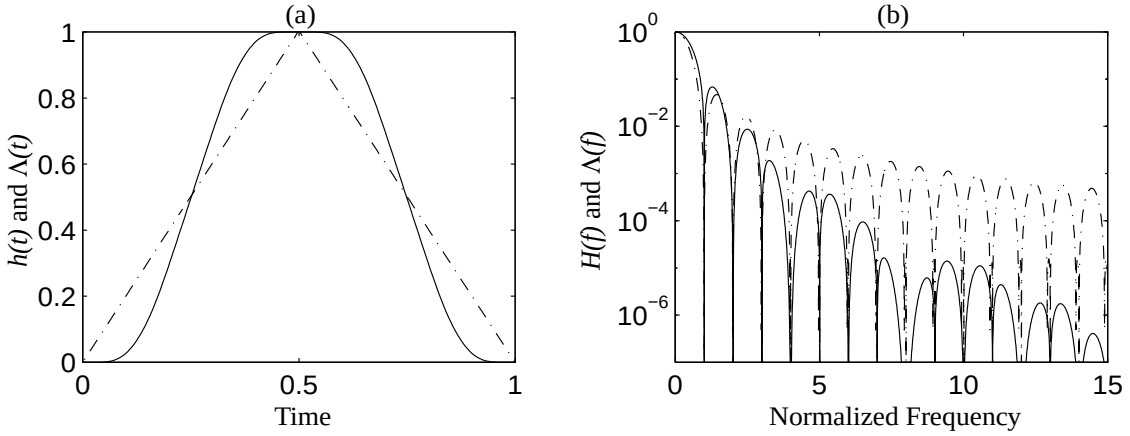

Figure 1. (a) Hut- and triangular function normalized to $T = 1$. (b) Spectra. (Solid: Hut; Dashed: triangle)

2) *(Complementary Baby)* Starting with a single one in each iteration a one is substituted by 10 and the number zero is substituted by 01, which yields $1; 10; 1001; 10010110; \ldots$

3) *(Append inverse)* Starting with a one in each step the sequence is doubled by append the inverse sequence to the original, e.g. from 10 we get 10-01=1001

The MTS is a *self generating, aperiodic* sequence which is in addition self-similar, because the sequence remains the same if we delete each second sample. In wavelet terminology the function is self-similar on the dyadic grid 2^k. If the time function is self-similar, than because of

$$f(t) = f(2^k t) \longleftrightarrow F(\omega) = 2^{-k} F(\omega 2^{-k}) \tag{2}$$

the spectrum is also self-similar. Figure 2(b) shows the FFT spectrum of the MTS for 16K data. If we compare the area 0-2000 and 0-4000, we can see the self-similar character of the spectrum. Of interest may also be a two dimensional arrangement of the MTS and we get an autostereogram.[7]

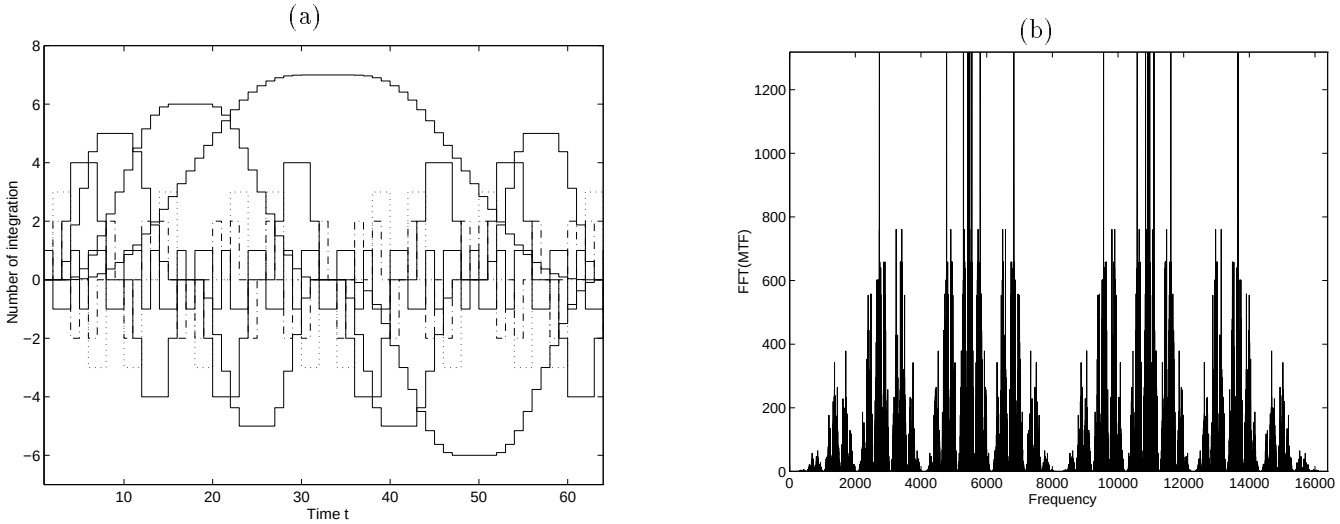

Figure 2. (a) Construction of the Hut function using the MTS. The function are normalized that the maximum of each function correspond with the number of integrations. (b) Spectrum of the MTS (FFT of 16K values).

Table 1. Comparison of different window.

	3 dB bandwidth	first zero	Maximum sidelobe	Asymptotic sidelobe decrease decrease each octave
Rectangular	$0.89/T$	$1/T$	-13 dB	-6 dB
Triangular	$1{,}28/T$	$2/T$	-27 dB	-12 dB
Hanning	$1{,}44/T$	$2/T$	-32 dB	-18 dB
Hut	$1{,}25/T$	$2/T$	-22 dB	$-\infty$ dB

There are several interesting applications of the Hut function. For instance Baker[8,9] shows that the asymptotic behaviour of an frequency modulated signals is given by

$$S(f) \sim f^{-(2c+6)} \tag{3}$$

where c is the number of continuos derivations of the base impulse $q(t)$ for which $q^{(c)}(0) = q^{(c)}(T)=0$ holds. As we can see from equation (1) we have for the Hut function $c = \infty$ and therefore an asymptotic infinity fast decrease in the spectrum.[6]

Window functions, like the triangular (Bartlett) window, are used in digital signal processing to reduce leakage, i.e. Gibb phenomenon, which occur by using a finite number of samples. This windows are typically characterised in the frequency domain. Table 1 shows the four most important parameter for the Hut function and some other common used windows. Again, like in digital FM, the asymptotic behaviour is unusual and should be verified. We review the computation of the asymptotic behaviour using the triangular window to clarify the computation. For the triangular window the quotient of the spectrum at 2ω and ω is

$$\lim_{\omega\to\infty} \frac{\Lambda(2\omega)}{\Lambda(\omega)} = \lim_{\omega\to\infty} \left(\frac{\operatorname{sinc}(2\omega)}{\operatorname{sinc}(\omega)}\right)^2 = \lim_{\omega\to\infty} \left(\frac{\sin(2\omega)}{\sin(\omega)}\right)^2 \cdot \frac{1}{4} \to \frac{1}{4} \tag{4}$$

and in logarithmic measurements we have

$$20\ \log \frac{\Lambda(2\omega)}{\Lambda(\omega)} = -12 \text{ dB each oktave} \tag{5}$$

For the Hut function we use the same algorithm. We used again the right side of equation (1) of the spectrum and compute then the limes for $\omega \to \infty$.

$$\lim_{\omega\to\infty} \prod_{i=0}^{\infty} \operatorname{sinc}\left(\frac{\omega}{2^i}\right) \to \lim_{\substack{\omega\to\infty \\ k\to\infty}} \prod_{i=0}^{k-1} \frac{2^i}{\omega} \quad = \quad \lim_{\substack{\omega\to\infty \\ k\to\infty}} \frac{2^{\frac{k(k-1)}{2}}}{\omega^k} \tag{6}$$

$$20\log \frac{H(2\omega)}{H(\omega)} = 20\log \lim_{\substack{\omega\to\infty \\ k\to\infty}} \frac{\frac{2^{\frac{k(k-1)}{2}}}{(2\omega)^k}}{\frac{2^{\frac{k(k-1)}{2}}}{\omega^k}} = 20\log \lim_{k\to\infty} 2^{-k} \to -\infty \text{ dB} \tag{7}$$

this means that the Hut spectrum has an asymptotically infinitely fast decrease in amplitude.

2. CONSTRUCTION OF THE HUTLET WAVELET FAMILY

We observe that the spectrum of the Hut function $H(\omega)$ looks like a the spectrum of a scaling function $\Phi(\omega)$,[10,1] used to construct wavelets. Wavelet construction typically begins with the scaling function $\phi(t)$, which can be expressed

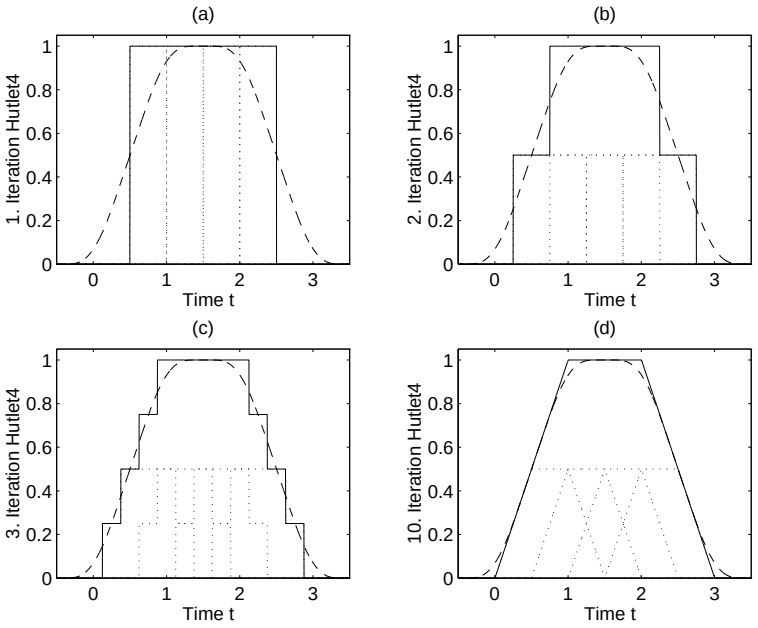

Figure 3. Iteration step 1,2,3, and 10 for the cascade algorithm construction of Hutlet4. (solid line $\phi(t)$; points $1/2\phi(2t-k)$; ideal Hut function dashes)

as a sum of self dilations and translations. If the discrete wavelet transform (DWT) is restricted to the usual dyadic grid (only scaling by a factor of two), and considering wavelets of finite support, the construction rule becomes

$$\phi(t) = \sum_{k=0}^{N-1} c_k \phi(2t-k) \quad \longleftrightarrow \quad \Phi(\omega) = \frac{1}{2}\sum_k c_k e^{-j\omega k/2}\Phi(\omega/2), \tag{8}$$

where $\sum_k (-1)^k c_k = 0$ ensures that there is no DC contribution in the multiscale analysis. The actual wavelet $\psi(t)$, also called mother wavelet, can then be calculated using

$$\psi(t) = \sum_{k=0}^{N-1} (-1)^k c_{N-1-k}\phi(2t-k) \quad \text{with} \quad \int \psi(t)\,\mathrm{dt} = 0. \tag{9}$$

The wavelet family therefore becomes $\phi_{n,k}(t) = 2^{-n/2}\phi(2^{-n}t-k)$ and $\psi_{n,k}(t) = 2^{-n/2}\psi(2^{-n}t-k)$ with $n,k \in \mathbb{N}$. This construction scheme can be applied to the Hut function given by Equation (1). First the spectrum of the Hut function, after shifting by $T/2$ to become causal, is given by

$$H_+(\omega) = H(\omega)e^{-j\omega T/2} \quad = \quad e^{-j\omega T/2}\prod_{i=1}^{\infty}\mathrm{sinc}(2^{-i}\omega T/2). \tag{10}$$

Applying Equation (8) to the causal Hut function, it is required that

$$H_+(\omega) \quad = \quad \frac{1}{2}\sum_k c_k e^{j\omega k/2}H_+(\omega/2) \tag{11}$$

$$\begin{aligned}\frac{H_+(\omega)}{H_+\left(\frac{\omega}{2}\right)} &= \frac{e^{-j\omega T/2}\mathrm{sinc}\left(\omega\frac{T}{4}\right)\mathrm{sinc}\left(\omega\frac{T}{8}\right)\mathrm{sinc}\left(\omega\frac{T}{16}\right)\cdots}{e^{-j\omega T/4}\mathrm{sinc}\left(\omega\frac{T}{8}\right)\mathrm{sinc}\left(\omega\frac{T}{16}\right)\mathrm{sinc}\left(\omega\frac{T}{32}\right)\cdots} \\ &= e^{-j\omega T/4}\mathrm{sinc}\left(\omega\frac{T}{4}\right) = \frac{1}{2}\sum_k c_k e^{-j\omega k/2}.\end{aligned} \tag{12}$$

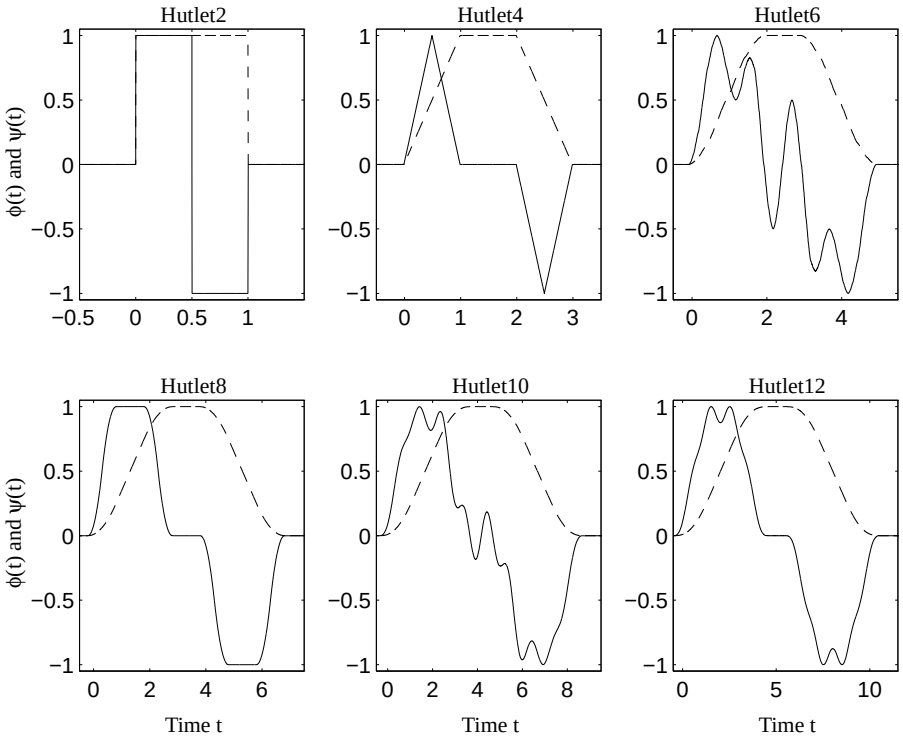

Figure 4. Mother wavelets $\psi(t)$ (solid line) and scaling functions $\phi(t)$ (dashed line) after ten iterations of the cascade algorithm. The amplitudes are normalized to one.

Substituting for $\omega/2$ by ω yields

$$e^{-j\,\omega T/2}\mathrm{sinc}(\omega T/2) \quad = \quad \sum_k c_k e^{-j\,\omega k}, \tag{13}$$

and finally the transformation back to the time domain yields

$$e^{-j\,\omega T/2}\mathrm{sinc}(\omega T/2) \quad \longleftrightarrow \quad \begin{array}{c} \frac{1}{T} \\ \sqcap \\ 0 \quad T \end{array} \quad = \quad \sum_{0 \le k < T} c_k\, \delta(t-k). \tag{14}$$

Equation (14) cannot be exactly realized with a finite number of coefficients, c_k. An approximation of the rectangles with N Dirac impulses with $c_k = 2/N$ gives a better approximation with increasing T and increasing number of coefficients. On the other hand the mother wavelet should be DC free, so only a even number of coefficients are used. To justify the use of a finite number of coefficients, the *cascade algorithm*

$$\phi^{(i+1)}(t) = \sum_{k=0}^{N-1} c_k \phi^{(i)}(2t-k) \tag{15}$$

will show the smooth [‡] convergence. For two coefficients $c_0 = c_1 = 1$, one obtains the Haar wavelet. For four coefficients $c_k = 1/2$, the construction of the Hutlet4 is shown in Figure 3. Starting with rectangle in the first iteration, it is shown that the cascade algorithm converges to a trapezoidal function. The wavelet, Hutlet4, is obtained from differences which gives two small triangles with opposite sign, as shown in Figure 4. For two to twelve, and even coefficients, Figure 4 shows all scaling functions and mother wavelets convergence after 10 iterations of the cascade algorithm. The difference between the scaling and Hut function becomes smaller as the number of coefficients increases (compare Figure 1 and Figure 4).

[‡] If the cascade algorithm converges to a rough function (e.g. a fractal) than the DWT produces blocking-like artifacts in the synthesis.[3]

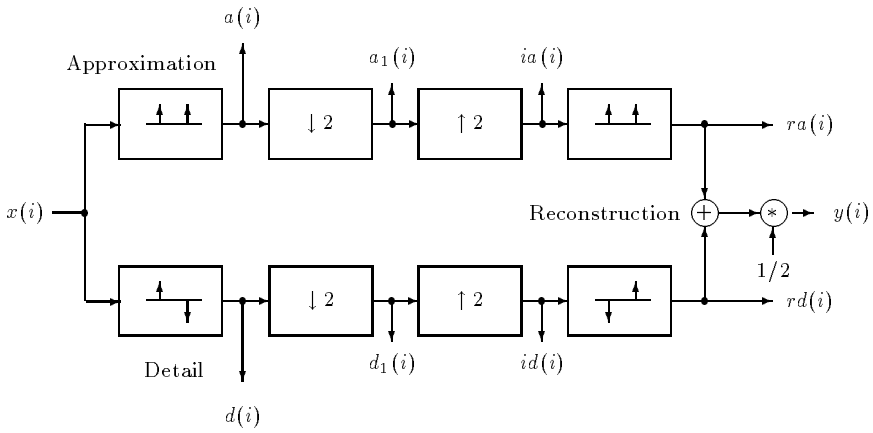

	Time step i				
	0	1	2	3	4
$x(i)$	x_0	x_1	x_2	x_3	x_4
$a(i)$	x_0	$x_0 + x_1$	$x_1 + x_2$	$x_2 + x_3$	$x_3 + x_4$
$d(i)$	x_0	$x_1 - x_0$	$x_2 - x_1$	$x_3 - x_2$	$x_4 - x_3$
$ia(i)$	x_0	0	$x_1 + x_2$	0	$x_3 + x_4$
$id(i)$	x_0	0	$x_2 - x_1$	0	$x_4 - x_3$
$ra(i)$	x_0	x_0	$x_1 + x_2$	$x_1 + x_2$	$x_3 + x_4$
$rd(i)$	$-x_0$	x_0	$x_1 - x_2$	$x_2 - x_1$	$x_3 - x_4$
$y(i)$	0	x_0	x_1	x_2	x_3

Figure 5. QMF for the Haar wavelet (Hutlet No. 2).

3. REALIZATION WITH QMF

In this section it will be shown that the Hutlets can efficiently be realized by the FSF explained in Sections II and III. An efficient implementation of the DWT uses QMF.[3,11,12] Obviously, the coefficients of the the scaling function $h_0(k) = c_k$ and the coefficients of the the mother wavelet $h_1(k) = (-1)^k c_{N-1-k}$ build lowpass and highpass filters, respectively.

Figure 5 exhibits the analysis and synthesis part for the Haar QMF. The analysis part consists of the lowpass and highpass filter and the decimator. The synthesis part consists of two interpolators, two reconstruction filters and a superposition of the two reconstructed signals. For the input sequence $x(i) = \{x_0, x_1, x_2, \ldots\}$, the moving average and moving difference are computed. The sum signals, shown in the Table of Figure 5 (for instance $a_1 = x_0 + x_1$), are normally computed and there is only one sequence value $a(i)$. After the splitting in approximation and detail signal by the lowpass and highpass, respectively, the sampling rate is reduced by a factor of two without loss of any information. As can be seen from the superposition of the sequences $ra(i)$ and $rd(i)$ is a *perfect* reconstruction without quantization error, even if the filters are realized with RNS integer arithmetic. In typical applications, like image compression, de-noising, or image enhancement, the QMF spitting is applied several times so that the analyzed signals are well represented (short and long-term) by the wavelet transforms.

It is well known from the literature that the only perfect reconstruction, linear phase, orthogonal QMF are trivial single or two tap filters.[10,13] With biorthogonal wavelets, perfect reconstruction *and* linear phase are possible. At first glance it would seem impossible to realize a perfect reconstruction for Hutlet of order higher than two. For instance, a moving average of four values and the moving difference of four values must be reconstructed. It can be seen from Figure 6, for Hutlet4, that this is nonetheless possible. The approximation filter and detail filter both have length four. Again decimation and interpolation by two forces each second sample to zero. The purpose of constructing the reconstruction filter was to realize the same reconstruction sequences $ra(i)$ and $rd(i)$ as for the Haar wavelet (see Figure 5). Each reconstruction filter can then be separately designed since the superposition at the output ensures perfect reconstruction. As shown in Figure 6, the reconstruction filters consist of the same structures

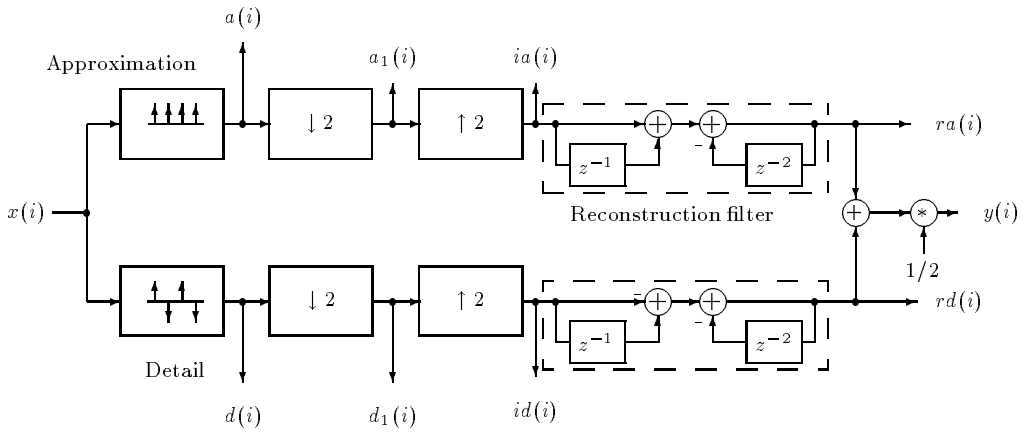

	Time step i				
	0	1	2	3	4
$x(i)$	x_0	x_1	x_2	x_3	x_4
$a(i)$	x_0	x_0+x_1	$x_0+x_1+x_2$	$x_0+x_1+x_2+x_3$	$x_1+x_2+x_3+x_4$
$d(i)$	x_0	x_1-x_0	$x_2-x_1+x_0$	$x_3-x_2+x_1-x_0$	$x_4-x_3+x_2-x_1$
$ia(i)$	x_0	0	$x_0+x_1+x_2$	0	$x_1+x_2+x_3+x_4$
$id(i)$	x_0	0	$x_2-x_1+x_0$	0	$x_4-x_3+x_2-x_1$
$ra(i)$	x_0	x_0	x_1+x_2	x_1+x_2	x_3+x_4
$rd(i)$	$-x_0$	x_0	x_1-x_2	x_2-x_1	x_3-x_4
$y(i)$	0	x_0	x_1	x_2	x_3

Figure 6. QMF for Hutlet No 4.

as the Haar filters in the first part, and a second recursive part which ensures that the partially reconstructed output values are subtracted from the internal sequence.

The use of different orthogonal analysis and synthesis filters results in a *biorthogonal* wavelet transfrom. Unfortunately, the synthesis filter are (nondecreasing amplitude) IIR filters and can not be iteratively constructed using the cascade algorithm. Nevertheless, by computing the upsampled version of $F(z)F(z^2)F(z^4)\cdots F(z^{2^{L-1}})$ it is possible to define the envelope of level L synthesis filter path.[3]

3.1. Generalisation to Any Even Length

Figure 7(a) shows how this principle can be extended to any even length. The approximation is a CIC lowpass from Hogenauer[14] while the detail filter is a CHPC and can be found in the Ph. D. thesis of the first author.[15] A generalisation of this type of efficient frequency sampling filters to higher order can be found in an other recent paper.[16] The complexity can be further reduced by interchanging the sequence of the decimation and comb sections, as shown in Figure 7(c). The same interchanging can be applied to the reconstruction filters, which is shown in Figure 7(b).

A graphical argument for perfect reconstruction, based on the Figures 6 and 7, will be proven for any Hutlet of even length. In general, the approximation filter $H_0(z)$ and detail filter $H_1(z)$ are geometric series given by

$$\text{Approximation} = H_0(z) \quad = \quad 1 + z^{-1} + \cdots + z^{-D+1} = \frac{1-z^{-D}}{1-z^{-1}} \tag{16}$$

$$\text{Detail} = H_1(z) \quad = \quad 1 - z^{-1} + \cdots - z^{-D+1} = \frac{1-z^{-D}}{1+z^{-1}}, \tag{17}$$

which are the first order single stage CIC and CHPC filter.[14–16] The reconstruction filter $F_0(z)$ for the approximation path is

$$F_0(z) \quad = \quad \frac{1+z^{-1}}{2} \cdot \frac{1}{1+z^{-2}+\cdots+z^{-D+2}} = \frac{1+z^{-1}}{2} \cdot \frac{1-z^{-2}}{1-z^{-D}}, \tag{18}$$

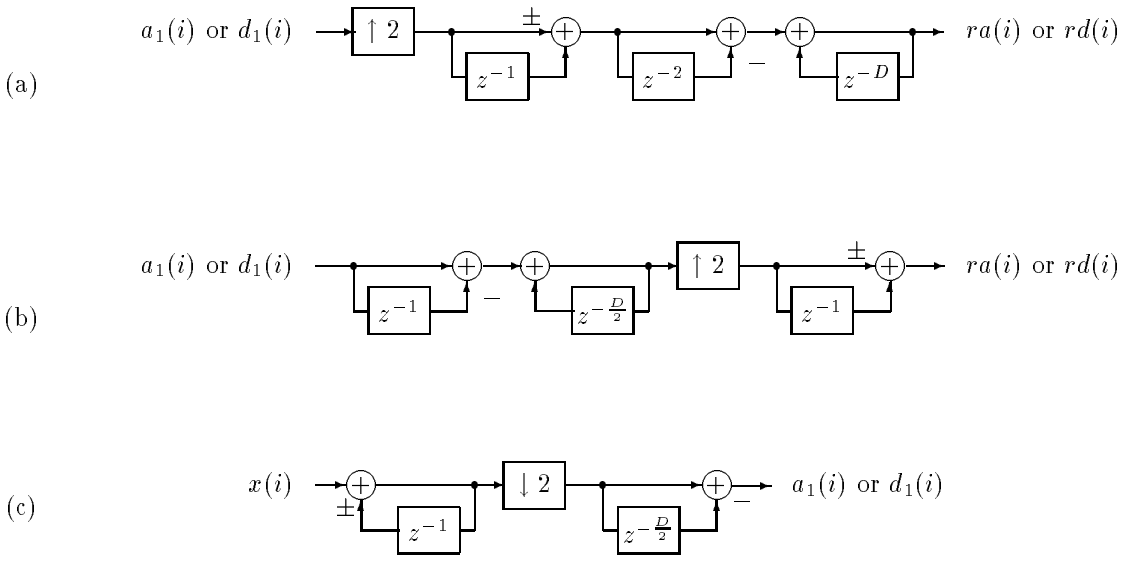

Figure 7. (a) Reconstruction filter QMF of any length. (b) Optimise reconstruction filter. (c) Optimise approximations- and detail-filter.

and the detail path becomes

$$F_1(z) \quad = \quad \frac{-1+z^{-1}}{2} \cdot \frac{1}{1+z^{-2}+\cdots+z^{-D+2}} = \frac{-1+z^{-1}}{2} \cdot \frac{1-z^{-2}}{1-z^{-D}}. \tag{19}$$

The overall transfer function for a two channel QMF bank (p. 105[3] or p. 380[12]) becomes

$$Y(z) \quad = \quad \frac{1}{2}\left(F_0(z)H_0(z)+F_1(z)H_1(z)\right)X(z) + \frac{1}{2}\left(F_0(z)H_0(-z)+F_1(z)H_1(-z)\right)X(-z).$$

Aliasing cancellation occurs for $F_0(z)H_0(-z)+F_1(z)H_1(-z)=0$. For even D, it follows that

$$2F_0(z)H_0(-z) = 1-z^{-2} \qquad 2F_1(z)H_1(-z) = -(1-z^{-2}). \tag{20}$$

The condition for *no distortion* is $F_0(z)H_0(z)+F_1(z)H_1(z) = 2z^{-l}$ where $l \in \mathbb{Z}$. It follows for even length Hutlets that

$$2F_0(z)H_0(z) = (1+z^{-1})^2 \qquad 2F_1(z)H_1(z) = -(1-z^{-1})^2 \tag{21}$$

$$F_0(z)H_0(z)+F_1(z)H_1(z) \quad = \quad 2z^{-1}. \tag{22}$$

From the *aliasing cancellation* and *no distortion* conditions it follows perfect reconstruction, is given by

$$Y(z) = X(z)z^{-1}. \tag{23}$$

4. APPLICATION OF THE HUTLETS: DETECTION OF ENVELOPE DISCONTINUITY IN AMPLITUDE MODULATION

The detection of discontinuities in signals using wavelets was popularized by S. Mallat.[17] The discontinuity appear as maxima or minima in the wavelet transforms. We will apply a multi-resolution analysis to an amplitude modulated signal. Knowledge of the exact time of the discontinuity in the envelope can, for instance, be used in the radio control watch signals (provided by WWVB in US, DCF77 in central Europe, and JG2AS in Japan) to extract exact

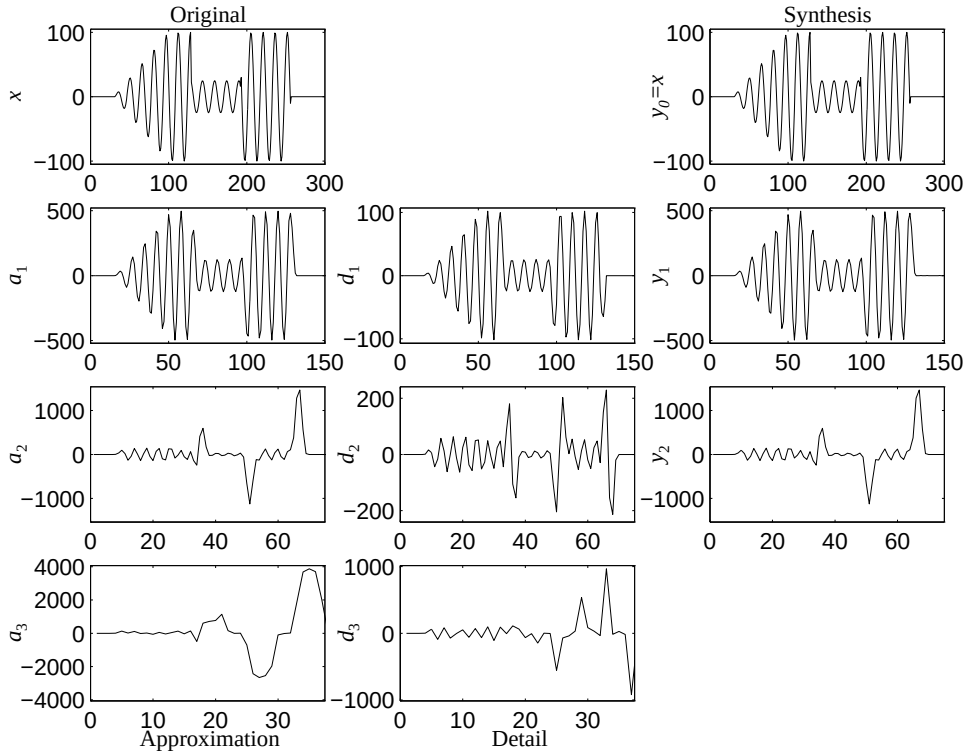

Figure 8. Analysis and synthesis of an amplitude modulated signal with Hutlet8.

time markers of each second. The detection of the discontinuities in a stepresponse is equivalent to the detection of the discontinuities in the envelope of an amplitude modulated signal. Compared to the complicated computation of the Lipschitz regularity by Mallat[17] the proposed method only requires the computation of the difference of two time shifted "moving averages". This is the function performed by the *detail* signals of the Haar DWT analysis. Strang and Nguyen[3] have shown that for high oversampling ratio, a Haar analysis gives sufficient accuracy in the detections. We will show by example that for medium to small oversampling ratios the Haar analysis gives too poor time resolution relative to a Hutlet analysis.

Figure 8 shows the original signal (left top), the approximation signals, and the detail signals for Hutlet8. The right column shows the perfect reconstruction using the signals a_3, d_3, d_2, and d_1. From the shape of the envelope of the "Original" signal, we expect at least three extreme (minima or maxima), according to the three discontinuities in the envelope of the amplitude modulated signal. Obviously, the discontinuity in the envelope can be easily observed in the signals a_2 or d_2 with a threshold detector. Here a_2 has three extremes, while each discontinuity in the envelope causes a biphase impulse within d_2.

The same analysis repeated for the Haar wavelet, shown in Figure 9, produced considerably poorer results. Clearly, there is a perfect reconstruction (right column), but there is only one maximum each in a_4 and d_4 observable. In addition, the time accuracy of the Haar analysis of a_4 and d_4 in Figure 9 is four times poorer than for Hutlet8 comparing a_4 and d_4 from the fourth level decomposition with the second level of a_2 and d_2 of the Hutlet8 analysis from Figure 8.

5. CONCLUSION

The paper describes first the various constructions scheme for the Hut function. We used the Hut function to construct a biorthogonal wavelet family, which are called Hutlets. A realization with perfect reconstruction, multiplier- free

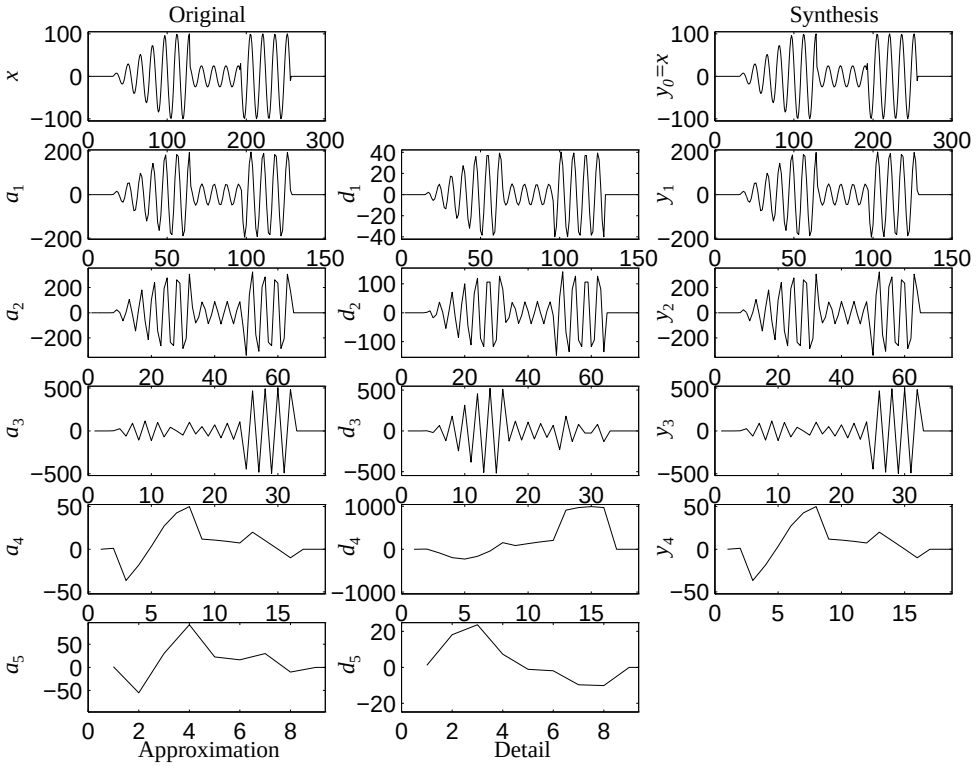

Figure 9. Analysis and synthesis of an amplitude modulated signal from example signal of 8 with Hutlet2 (Haar wavelet).

quadrature mirror filters using RNS technic was discussed. The approximation-filter was a CIC lowpass, the detail-filter was a CHPC highpass, and the reconstruction filters were IIRs. An application of the Hutlets has shown superior properties compared with the Haar wavelet in the detection of envelope discontinuity in amplitude modulation signals.

ACKNOWLEDGEMENTS

The first author would like to thank Prof. Hilberg for introducing the Hut function to him in 1990. We would also like to thank our colleagues from the University of Florida, Dr. I. Koren, Dr. A. Lain, and Dr. J. Mellott for valuable discussions. We also like to thank the "Deutsche Forschnungsgemeinschaft" for the support under grant ME1419/2-1.

APPENDIX A. FUNCTIONAL APPROXIMATION OF THE HUT FUNCTION

The construction of the Hut function using the MTS or the iterative convolution works well for sequence length 2^k. It may therefore be useful to have additional functional approximation for any length. The Taylor sequence and Fourier sequence have been known since same time.[4] Two computer friendly constructions should also be mentioned.[6] The Taylor sequence of the Hut function can be constructed using the differentiation rule of the Hut function $f'(x) = f(2x)$ which yields[4]:

$$h(x) \quad = \quad \sum_{n=0}^{\infty} a_n x^n = \sum_{n=0}^{\infty} \frac{2^{\frac{(n-1)n}{2}}}{n!} x^n. \tag{24}$$

A second approximation uses the Fourier series, where the Hut function has a periodic extension, i.e.

$$\sum_{k=0}^{\infty} a_k \cos(\frac{2\pi}{T} k x) \tag{25}$$

Table 2. (a) Fourier series coefficients. (b) Coefficients for the Tschebyscheff approximation.

(a)

Coefficients			
a_0	0.5	$\cdot$	10^0
a_1	0.553770	$\cdot$	10^0
a_3	-4.620147	$\cdot$	10^{-2}
a_5	-8.656431	$\cdot$	10^{-3}
a_7	1.044698	$\cdot$	10^{-3}
a_9	-3.561026	$\cdot$	10^{-4}
a_{11}	2.982849	$\cdot$	10^{-4}
a_{13}	9.136547	$\cdot$	10^{-5}
a_{15}	-6.557784	$\cdot$	10^{-6}

(b)

symmetric	asymmetric
$2b_0 = 0.68197$	$2b_0 = 1.00012$
$b_2 = -0.51495$	$b_1 = -0.59846$
$b_4 = 0.19594$	$b_3 = 0.11848$
$b_6 = -0.00236$	$b_5 = -0.01983$
$b_8 = -0.02822$	$b_7 = -0.00185$
$b_{10} = 0.01143$	$b_9 = 0.00220$
$b_{12} = -0.00612$	$b_{11} = -0.00080$
$b_{14} = 0.00552$	$b_{13} = 0.00045$
$b_{16} = -0.00306$	$b_{15} = -0.00029$
$b_{18} = 0.00078$	$b_{17} = 0.00012$
$b_{20} = 0.00036$	
$b_{22} = -0.00044$	
$b_{26} = 0.00022$	
$b_{28} = -0.00012$	

This approximation gives also a much faster convergence than the Taylor series. Table 2(a) shows Fourier series coefficients up to a_{15}. The third approximation to discuss is the Bessel function approximation using

$$h(x) = \frac{1}{1 + (\frac{x}{T/4})^n} \tag{26}$$

We use 300 iteration in the "Downhill" method of Nelder and Mead[18] to optimize the exponent n for 32K Hut field. If we use the point symmetry regarding $T/4$ than the maximum error norm l_∞ is only 0.2 percent. Figure 10 shows the approximation, while the following table shows the mean and maximum error $\varepsilon_r = y_r - f(x_r)$ where $f(x_r)$ is the ideal values and y_r is the approximation value:

	$[0, \frac{T}{4}]$	$[\frac{T}{4}, \frac{T}{2}]$
Exponent: n	3.74582	5.96823
$\frac{4}{m}\sum_{r=1}^{m/4} \lvert\varepsilon_r\rvert$	$1.11 \cdot 10^{-3}$	$2.60 \cdot 10^{-2}$
$\mathrm{MAX}\lvert\varepsilon_r\rvert$	$2.15 \cdot 10^{-3}$	$3.21 \cdot 10^{-2}$

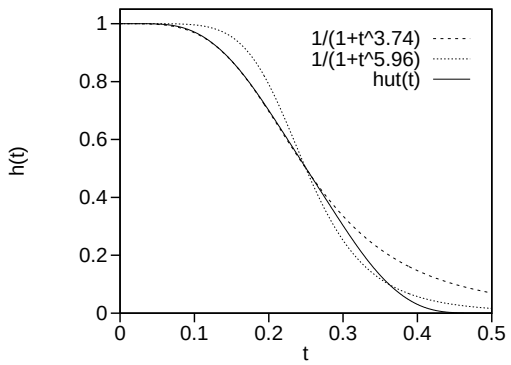

(a)

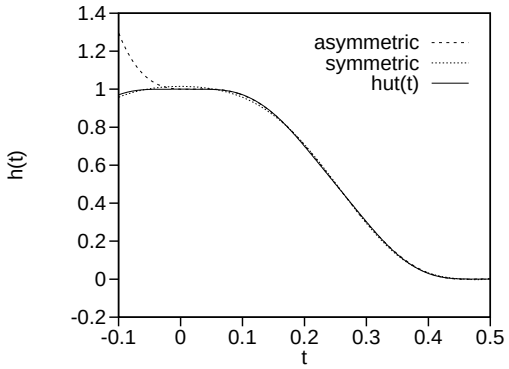

(b)

Figure 10. (a) Hut function approximation through Bessel functions using exponent $n = 3.74582$ and $n = 5.96823$ ($t = x/T$). (b) Tschebyscheff approximation for four coefficients b_0, b_1, b_3 and b_5 for the *asymmetric* approximation and b_0, b_2, b_4 and b_6 for the *symmetric* approximation.

It's well known from approximation theory that for the l_∞ norm the Tschebyscheff approximation[18] gives the optimum result. To apply the Tschebyscheff approximation we have first to transform the range $[a,b]$ to $x \in [-1,1]$ with $x = (2x' - b - a)/(b - a)$. Now we can use an iterative algorithm[18] to compute the coefficients of

$$f(x) = \sum_{i=0}^{k-1} b_i T_i(x). \tag{27}$$

with $T_k(x)$ being the Tschebyscheff polynomials

$$\begin{array}{lll} T_0(x)=1 & T_1(x)=x & T_2(x)=2x^2-1 \\ T_3(x)=4x^3-3x & T_4(x)=8x^4-8x^2+1 & T_5(x)=16x^5-20x^3+5x \end{array}$$

or in general

$$T_{k+1}(x) = 2xT_k(x) - T_{k-1}(x) \tag{28}$$

For a symmetric function to the ordinate axis all odd b_i are zero, and for an asymmetric function to (0,1) all even coefficients are zero. Table 2(b) shows the Tschebyscheff coefficients for symmetric and asymmetric Hut functions and Figure 10(b) shows approximation with four coefficients. The error for four coefficients become $l_\infty = 0.0053222$ for the asymmetric approximation and $l_\infty = 0.051877$ for the symmetric approximation. If we use *all* coefficients from Table 2(b) (where only value greater 10^{-4} are shown) the error bounds become $l_\infty = 0.000091$ for the asymmetric approximation and $l_\infty = 0.000412$ for the symmetric approximation.

REFERENCES

1. S. Mallat, "A theory for multiresolution signal decomposition: The wavelet representation," *IEEE Transactions on Pattern Analysis and Machine Intelligence* , pp. 674–693, July 1989.
2. M. Vetterli and J. Kovacevic, *Wavelets and Subband Coding*, Prentice Hall, 1995.
3. G. Strang and T. Nguyen, *Wavelets and Filter Banks*, Wellesley-Cambridge Press, 1996.
4. W. Hilberg, "Impulse und Impulsfolgen, die durch Integration oder Differentiation in einem veränderten Zeitmaßtab reproduziert werden," *Arch. für Eltr. Übertr. (AEÜ)* **25**, pp. 39–48, 1971.
5. M. Schroeder, *Number Theory in Science and Communication*, Springer–Verlag, 1986.
6. U. Meyer-Bäse, "Spektrale Betrachtungen zur Hut-funktion und mögliche Anwendungen in der digitalen Signalverarbeitung," tech. rep. 134, Institute for Data Technic, TU Darmstadt, 1991.
7. W. Hilberg, "Mehrdimensionale Morse-Thue-Folgen," *Physik in unserer Zeit* **22**, pp. 24–28, 1991.
8. J. Anderson, T. Aulin, and C.-E. Sundberg, *Digital Phase Modulation*, Plenum Press, 1986.
9. T. Baker, "Asymptotic behavior of digital FM spectra," *IEEE Transactions on Communications* , pp. 1585–1594, Oct. 1994.
10. I. Daubechies, "Orthonormal bases of compactly supported wavelets," *Communications on Pure and Applied Mathematics* **XLI**, pp. 909–996, 1988.
11. M. Vetterli and Herley, "Wavelets and filter banks: Theory and design," *IEEE Transactions on Signal Processing*, pp. 2207–2232, Sept. 1992.
12. R. Crochiere and L. Rabiner, *Multirate Digital Signal Processing*, Prentice Hall, 1983.
13. P. Vaidyanathan, "Multirate digital filters, filter banks, polyphase networks, and applications: A tutorial," *Proceedings of the IEEE* , pp. 56–93, Jan. 1990.
14. E. B. Hogenauer, "An economical class of digital filters for decimation and interpolation," *IEEE Transactions on Acoustics, Speech and Signal Processing* , pp. 155–162, Apr. 1981.
15. U. Meyer-Bäse, *Der Einsatz komplexer Algorithmen zur Realisierung universeller Abtastempfänger in FPGA–Technik (The Use of Powerful Algorithms in the Realisation of Universal Sampling Receivers in FPGA Technics), VDI-press , Reihe 10, Nr. 404.* Ph.D. thesis, TU Darmstadt, 1995.
16. U. Meyer-Bäse, J. Mellott, and F. Taylor, "Design of RNS frequency sampling filter banks," *ICASSP, Session DSP1P* , 4 pages, Apr. 1997. (accepted for publication).
17. S. Mallat and W. Hwang, "Singularity detection and processing with wavelets," *IEEE Transactions on Information Theory* , pp. 617–643, Mar. 1992.
18. W. H. Press *et al.*, *Numerical Recipes in C*, Cambride University Press, 1992.